ADVANCES IN ATMOSPHERIC SCIENCES, VOL. 30, NO. 1, 2013, 193–209

Impacts of Polar Vortex, NPO, and SST Configurations on Unusually Cool Summers in Northeast China. Part I: Analysis and Diagnosis

LIAN Yi[1,2] (廉 毅), SHEN Baizhu[1,2] (沈柏竹), LI Shangfeng*[1,2] (李尚锋), ZHAO Bin[5] (赵 滨), GAO Zongting[1,2] (高枞亭), LIU Gang[1,3] (刘 刚), LIU Ping[1,3,4] (刘 平), and CAO Ling[4] (曹 玲)

[1] *Laboratory of Research for Middle–High Latitude Circulation Systems and East Asian Monsoon, Changchun* 130062

[2] *Institute of Meteorological Sciences of Jilin Province, Changchun* 130062

[3] *Jilin Meteorological Science and Technology Service Center, Changchun* 130062

[4] *Center of Weather Film in Jilin Province, Changchun* 130062

[5] *National Meteorological Center, Beijing* 100081

(Received 7 January 2012; revised 7 March 2012)

ABSTRACT

This study unveils the evolution of two major early signals in the North Pacific atmosphere–ocean system that heralded abnormal high-pressure blockings and cold-vortex activities across Northeast China, based on an analysis of the configurations of major modes including the polar vortex, the North Pacific Oscillation (NPO), and SST in the preceding winter and spring and atmospheric low-frequency disturbances in Northeast China. We analyzed these aspects to understand the atmosphere–ocean physical coupling processes characterized by the two early signals, and here we explain the possible mechanisms through which dipole circulation anomalies affect the summer low-temperature processes in Northeast China. We further analyzed the interdecadal variation background and associated physical processes of the two early signals.

Key words: polar vortex, NPO, North Pacific SST, atmosphere–ocean coupling, summer low temperatures in Northeast China, dipole pattern

Citation: Lian, Y., B. Z. Shen, S. F. Li, B. Zhao, Z. T. Gao, G. Liu, P. Liu, and L. Cao, 2013: Impacts of polar vortex, NPO, and SST configurations on unusually cool summers in Northeast China. Part I: Analysis and diagnosis. *Adv. Atmos. Sci.*, **30**(1), 193–209, doi: 10.1007/s00376-012-1258-x.

1. Introduction

The interaction between the ocean and the atmosphere is an important subject of global climate dynamics. The North Pacific Ocean and the Eurasian continent have the most extensive ocean–land connections in the world. In this context, the atmosphere–ocean coupling processes and their associated teleconnections, as well as their impacts on climate variations, have attracted much attention. Bjerknes (1966, 1969) first proposed the concept of El Niño-Southern Oscillation (ENSO) that shows a major link with global climate anomalies in the form of atmosphere–ocean teleconnections. Rogers (1981) pinpointed a North Pacific Oscillation (NPO), similar to the North Atlantic Oscillation (NAO). Wallace and Gutzler (1981) summarized the western Pacific (WP) teleconnection pattern, an upper-level teleconnection version of the NPO. Some studies have revealed a teleconnection wave train that travels in a large circular path between

*Corresponding author: LI Shangfeng, ice-lsf@163.com

the North Pacific and the North American continent (PNA; Namias, 1951; Klein, 1952; Wallace and Gutzler, 1981). Knowledge of atmosphere–ocean teleconnections in the North Pacific region has improved, especially since Madden and Julian (1971, 1972) discovered the 40-day low-frequency oscillation (LFO). Some regional circulation anomalies might be the result of a string of dynamic processes, including the forcing both in and outside of the region and the nonlinear interactions between waves and currents. The presence of the Pacific–Japan Oscillation (PJO) is closely associated with convective activities over the western equatorial Pacific or ENSO events. Huang and Li (1988) held that the PJ wave train that collided with North America via East Asia is directly associated with the convection heating in the Philippines area. He also proposed an East Asia/Pacific (EAP) teleconnection pattern, in an attempt to demonstrate the intervariation within the western Pacific subtropical high, the meiyu trough, and the Northeast Asia high (Huang and Li, 1987; Huang and Sun, 1992; Yang and Sun, 2005, Yang et al., 2005, Liang et al., 2011).

Attentions has been given to the possible linkage between the North Pacific atmosphere–ocean system and the unusually cool summers in Northeast China since the 1980s. Li (1989) reported a negative anomaly center above Northeast China in an El Niño summer, which contributes to the lower-than-normal temperature in the region. Zhang (1990) also indicated that El Niño results in the lower-than-normal temperature in the Northeast region. Other studies, however, have shown that in the 1950s–1970s, Changchun has an unusually cool summer if El Niño warming commences from the first half of the year (Lian and An, 1998). However, in the period 1980–1995, Changchun reported a higher or slightly higher than normal temperature pattern in summer, which had to be explained by the differed interseasonal oscillations staged by El Niño and outgoing longwave radiation (OLR; Lian and An, 1998). Zheng and Ni (1999) pointed out that the unusually cool summer in Northeast China had a decadal connection with ENSO events. Sun and Wang (2006) also confirmed this finding. In addition, scientists have begun to investigate the possible impacts of a polar vortex and NPO on climate in China, assembling a range of facts to make the teleconnections evident between the polar vortex and unusually cool summers in the Northeast, and between the NPO phases in the preceding winter and the summer atmospheric circulations, including Hadley circulation and precipitation distribution in China (Zhang et al., 1985; Zhao and Liao, 1992; Peng and Zhang, 1998; Liu et al., 2002, 2003; Lian, 2007; Zhou et al., 2008).

In 2009, both Jilin and Heilongjiang, two provinces in Northeast China, reported an unusually cool summer (cooler than any in the prior 15 years), with most of the two provinces reporting an averaged temperature anomaly exceeding -0.5°C (National Climate Center, 2010). The cool temperatures jeopardized local food production, especially the rice yield, which drew additional public attention again (Shen et al., 2011).

This study investigated the configuration of the polar vortex and NPO with North Pacific westerly drifts and ENSO phase, from the perspective of the interactions between the spring polar vortex and high-latitude atmosphere–ocean system, based on the two typical Northeast China summer low temperature incidences that occurred in 1964 and 1993. In this study, diagnosis analysis was applied to analyze the fact that the opposite early signals given by the two examples in the spring surprisingly yielded a remarkably similar sophisticated story, where high blocking and diversified abnormal cold vortex activities prompted the occurrence of an unusually cool summers in the Northeast China. Herein, the so-called "spring forecast threshold" is explained, and the physical mechanisms of high-low incidences that allow the mid- and high-latitude atmosphere–ocean coupling processes to stage a sustained cool summer decadal variation period in the Northeast China are revealed. The numerical modeling results will be presented in Part II of this study.

2. Data and calculation method

In this study, the 1948–2009 global reanalysis data was acquired from the National Centers for Environmental Prediction/National Center for Atmospheric Research (NCEP/NCAR), the 1958–2002 reanalysis was provided by the European Center for Medium-Range Weather Forecast (ECMWF), and the 1881–2005 SST data from the Meteorology Office of the Hadley Centre for Climate Change. According to the time scale defined by Shen et al. (2011) for classifying the extreme summer low-temperature events in Northeast China, a grade A cool summer event (i.e., serious) was defined as $\overline{T}_{6-8} \leqslant -1.0\sigma$ ($\overline{T}_{6-8}$ stands for the summer mean temperature of Changchun observatory station, σ represents standard deviation) observed at a weather station in the region; likewise, a grade B cool summer event was defined as $-1.0\sigma < \overline{T}_{6-8} \leqslant -0.4\sigma$. Both Changchun and Harbin were chosen as typical representatives of the temperature variation patterns in Northeast China (Lian and An, 1998). The summer of 1964, a cool summer event A, was chosen as a typical high-incidence example for diagnosis, and the summer of 1993, a cool summer event B, was chosen as a typical low-incidence example, based on the periodical

variations of cold and warm events (high and low incidence of low temperature events) over the past 30–40 years recorded by two weather stations at which surface temperature observations were made for at least the prior 100 years (Lian and An, 1998; Shen et al., 2011).

The 500-hPa height field harmonic analysis (Chou, 1985) was applied to analyze the low-frequency variations of super-longwave perturbation that contributed to the blocking-high and cold-vortex activities in Northeast China (Lian et al., 2010). The band-pass filter used by Li (1990) was applied to calculate the 30–60-day low-frequency oscillations in the 500-hPa vorticity field. The Rossby wave energy dispersion process was analyzed using the approach developed by Bueh and Nakamura (2007). Meanwhile, singular value decomposition (SVD) was employed for related analyses (Demmel and Kahan, 1990).

The polar vortex activity area index was calculated based on the formula and parameters given by Liu (1986). The target Pacific region covers an area from 150°E to 120°W. The Pacific-sector polar vortex area on the 500-hPa isobaric surface starts north of the contour bearing the signature of a polar vortex boundary to the pole:

$$S = \int_{\varphi}^{\frac{\pi}{2}} \int_{\lambda_1}^{\lambda_2} R^2 \cos\varphi d\varphi d\lambda = R^2(1-\sin\varphi)(\lambda_2-\lambda_1) , \quad (1)$$

which can be calculated per 10° longitude in a differential format. Here, R stands for the Earth' s radius at 6378 km, the units of S are 10^5 km, φ represents latitude, λ represents longitude. Based on different regions, the indices of polar vortex area S were divided into five categories as follows:

when $\lambda_1 = 0°, \lambda_2 = 360°$, and S is the index of Northern Hemisphere polar vortex area;

λ_1=60°, λ_2=150°, and S is the index of Asian polar vortex area;

λ_1=240°, λ_2=330°, and S is the index of North America polar vortex area;

λ_1=330°, λ_2=420°, (i.e., region covering from 30°W to 60°E, in an anticlockwise direction.), and S is the index of Atlantic and European polar vortex area;

λ_1=150°, λ_2=240°, and S is the index of the Pacific polar vortex (PPV) area.

The definition area and indexes of the Northeast Cold Vortex (NCV) and the NPO can be found in the work of Zhao and Liao (1992) and Liu et al. (2003); and the definition area of the central and western Asian blocking highs can be found in the work of Liu et al. (2012). The westerly drift zone was confined to an area from 150°E–150°W to 30°–46°N.

The NCV was defined as follows: over the region (35°–60°N, 115°E–145°W), there is at least one closed contour on 500-hPa geopotential height, accompanied a cold center or cold trough, and it maintains this state for at least three days within the defined domain. The blocking high was defined as follows: There is a center of high pressure on 500-hPa geopotential height, and the position of the center moves <2.5 times the meridian distance each day; moreover, the high-pressure center is maintained for at least three days.

The index of $\mathrm{NPO_L}$ (L was the abbreviation for the family name of "LIAN Yi") was defined as follows:

$$\mathrm{NPO_L} = P_{\mathrm{S1}} - P_{\mathrm{S2}} , \quad (2)$$

P_{S1}, P_{S2} means the area average of standardized sea surface pressure over the domain of (25°–40°N, 140°E–150°W) and (50°–65°N, 140°E–150°W).

The westerly drift index W was defined as follows: $W = A_{\mathrm{sst}}$ where A_{sst} is the area average of standardized SST over the domain (30°–46°N, 150°E–150°W).

The NAO index (NAOI) was defined as the difference in the normalized monthly sea level pressure (SLP) regionally zonal-averaged over the North Atlantic sector from 80°W to 30°E between 35°N and 65°N (Li and Wang, 2003).

The statistical significance of a composite difference was assessed using the Student's t-test. The 95% confidence level was considered significant, unless otherwise stated.

3. Connections between the PPV and NPO seasonal evolution

3.1 *Weak or strong anomalies for the spring PPV area*

Four typical weak and four typical strong years were selected separately from the spring PPV area index series. Strong years (1984, 1993, 1996, and 2005) reported an averaged anomaly of $\geqslant 15\times10^5$ km^2, whereas the weak years (1948, 1964, 1967, and 2002) reported an averaged anomaly of $\leqslant -20\times10^5$ km^2.

Figure 1a shows that the 500-hPa height-anomaly differences between four strong minus four weak years in the preceding winter formed in a pattern that features positive anomalies above the Aleutian Islands and negative anomalies on the southern flank of the North Pacific sector, a typical NPO-like negative phase. However, the 500-hPa height-anomaly differences (four years) depicted an entirely opposite picture against the preceding winter (Fig. 1b); they ended up in a north–south "−, +" distribution, suggesting a strong North PPV area, favoring an NPO-like positive phase.

The weak and strong PPV areas in the spring underwent a composite 1000-hPa wind anomalies dominated by the cyclonic circulation stretching from the

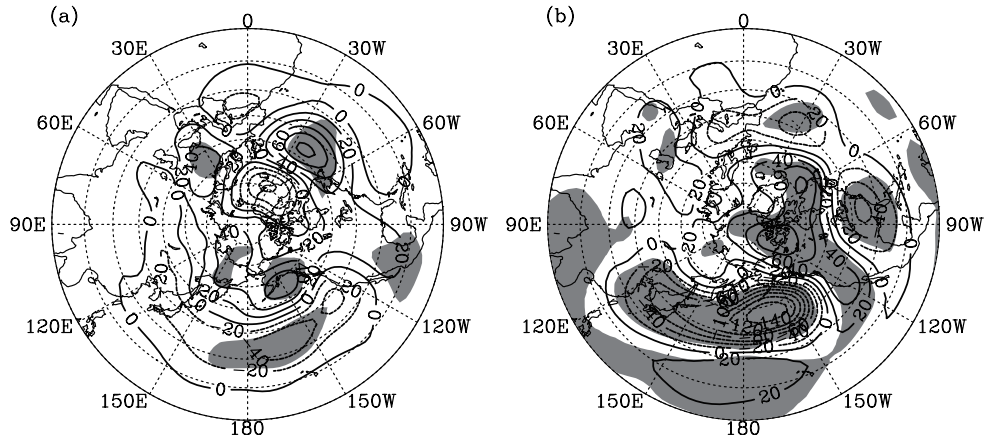

Fig. 1. Differences in 500-hPa height anomalies between four strong and four weak years: (a) the preceding winter, and (b) the following spring. Dotted lines represent the negative values, and shaded area indicates height anomalies beyond the 95% confidence level. Contour intervals are 20 gpm.

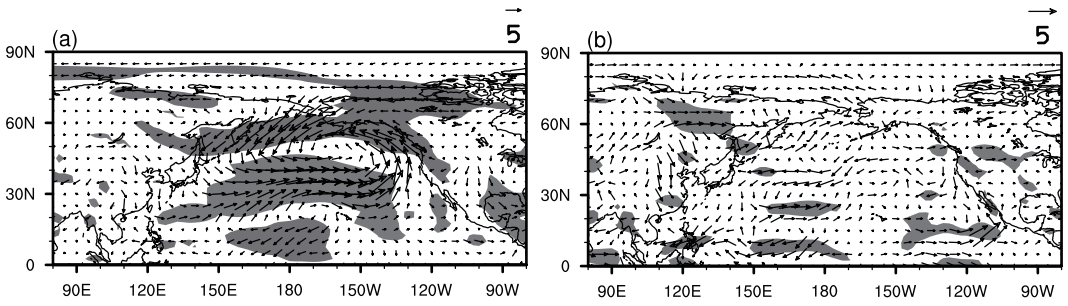

Fig. 2. Composite patterns of 1000-hPa wind anomaly differences between four strong and four weak years. Shaded area indicates the region of wind anomalies beyond the 95% confidence level. (a) the following spring, (b) summer (units: m s^{-1}).

Aleutian Islands in the center to the entire area north of 35°N over the North Pacific in a significant positive NPO phase, which in turn brought a significant westerly belt between 25°N and 40°N (Fig. 2a). The spring season weak and strong PPV areas weakened somewhat at the 1000-hPa wind fields in the summer, mainly dominated by an anticyclonic circulation stretching from west of the Aleutian Islands to the Sea of Okhotsk. Meanwhile, the north eastern and eastern parts of China were dominated by a strong northerly flow, which featured a weak summer monsoon but strong northerly cold air (Fig. 2b).

3.2 *Main mode configuration of spring NPO and North Pacific SST*

The spatial and temporal distribution of spring North Pacific SST and sea surface pressure SVD1 are shown in Fig. 3. The mode accounted for 61% of the squared covariance and total contribution, with a field correlation coefficient of 0.74. These distributions indicate that the North Pacific SST is configured with the central and eastern equatorial Pacific La Niña phase and the warm westerly drift zone phase in the northwest, in line with the north-to-south SLP "+, −" wave train, or with the major coupled mode of negative NPO phases. Likewise, the North Pacific SST is configured with the central and eastern equatorial Pacific El Niño phase and the cold westerly drift zone phase in the northwest, in line with the north-to-south SLP "+, −" wave train, or with the major coupled mode of positive NPO phases. As far as the time coefficient trends are concerned, the two fields mostly ran opposite in phase distribution except the 1960s. The North Pacific SLP in the north, with the Aleutian Islands at the center, has been dominated by a low-pressure system since 1976–77, when the Aleutian low suddenly strengthened in the winter. On the southern flank (a subtropical region), the SLP was mainly under the influence of high-value pressure systems. As a result, NPO entered a decadal variation period dominated mainly by a positive phase. Correspondingly, North Pacific sea surface temperature anomaly

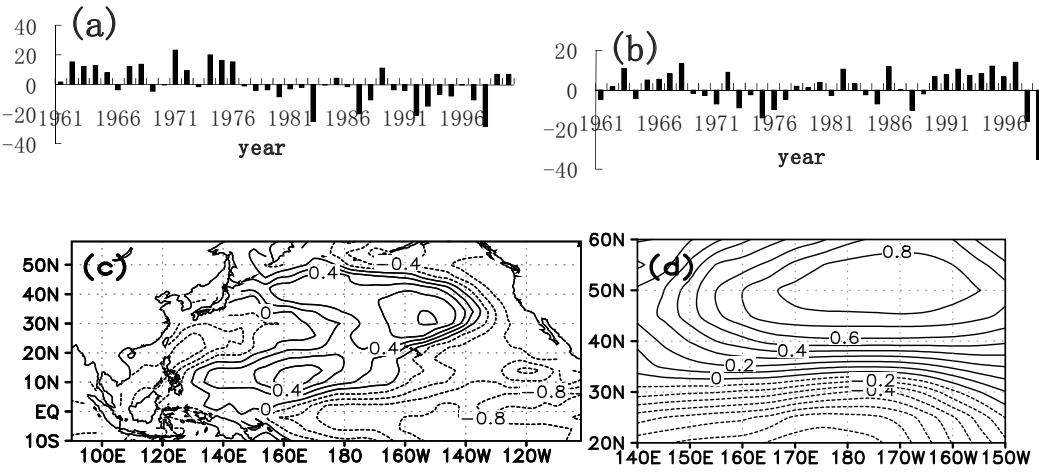

Fig. 3. Distribution of spring North Pacific SST (left) and sea-level pressure (right) in the same season and associated time coefficients: (a) and (b) show time coefficients, and (c) and (d) show distributions.

(SSTA) have been dominated by the cold northwest drift zone phase in the north since 1976, with the central and eastern equatorial Pacific under an El Niño phase, which agreed with the Pacific Decadal Oscillation (PDO) warm-phase analysis made by Mantua et al. (1997).

For five typical years with deepened spring Pacific Aleutian lows (1980, 1998, 1991, 1981, and 1987) and weakened spring Pacific Aleutian lows (1989, 1964, 1976, 1972, and 1967), based on SVD1 time coefficients, the real strength of Aleutian low and NPO index were chosen. Then composite SST and wind anomalies were analyzed. Our results are presented in the next section.

Figure 4a depicts the composite sea-surface wind and temperature anomalies for five individual years with deepened North Pacific Aleutian lows. The deepened northern Pacific Aleutian low bred out an equatorial northwesterly flow, or even a westerly flow over east of 155°E, which weakened the Walker circulation. The deepened Aleutian low in the spring also led to the convergence of prevailing westerly jets in the eastern Pacific westerly drift zone (35°–45°N) in the south and the northwesterly north 45°N to the west, forcing the westerly drift zone SSTA to remain in a cold phase. Five individual years with weakened northern Pacific Aleutian lows (Fig. 4b) had a composite sea surface wind and temperature anomaly running just opposite in distribution, with easterly jet prevailed over the westerly drift zone, and hence a warm SSTA phase, and the southeasterly over the equatorial zone east of 155°E, was favorable for a strengthened easterly under the Walker circulation. In Fig. 4c, a cold SSTA phase in the westerly drift zone and a warm SSTA phase in the central-eastern equatorial Pacific ocean can be clearly seen. Our analysis confirms the rationality of the aforementioned coupled atmosphere–ocean SVD1 mode, as well as the dynamic role played by sea-level pressure in defining SSTA fields.

In this section, a composite analysis and the SVD method were employed to reveal the major mode configuration of the PPV, NPO, and northern Pacific SST (the westerly drift zone, ENSO phase), in an attempt to sort out the strong and weak spring Pacific sector polar vortex area that contributes to positive and negative NPO phase anomalies at the mid-troposphere and in SLP. Meanwhile, positive or negative NPO phase anomalies often agreed with the first coupled mode that enjoys a stable westerly drift zone SST cold and warm phase and a similarly stable El Niño or La Niña phase (i.e., SVD1 accounted for 60% of the squared covariance and total contribution). This conclusion was further confirmed by the composite sea surface wind and temperature anomalies in a typical year with deepened and weakened spring Pacific Aleutian low.

4. Seasonal evolution of two early signals and associated atmospheric low-frequency variations

We analyzed the basic mode configuration of atmosphere–ocean systems in the early stage and the associated seasonal evolution for cool summer years based on two cities (Changchun and Harbin) that reported significant unusually cool summers in two typical years featuring either a high (1964) or low (1993) incidence of cool summers on a decadal background. The diagnosis of the seasonal evolution of two different early signals and their associated mid-troposphere

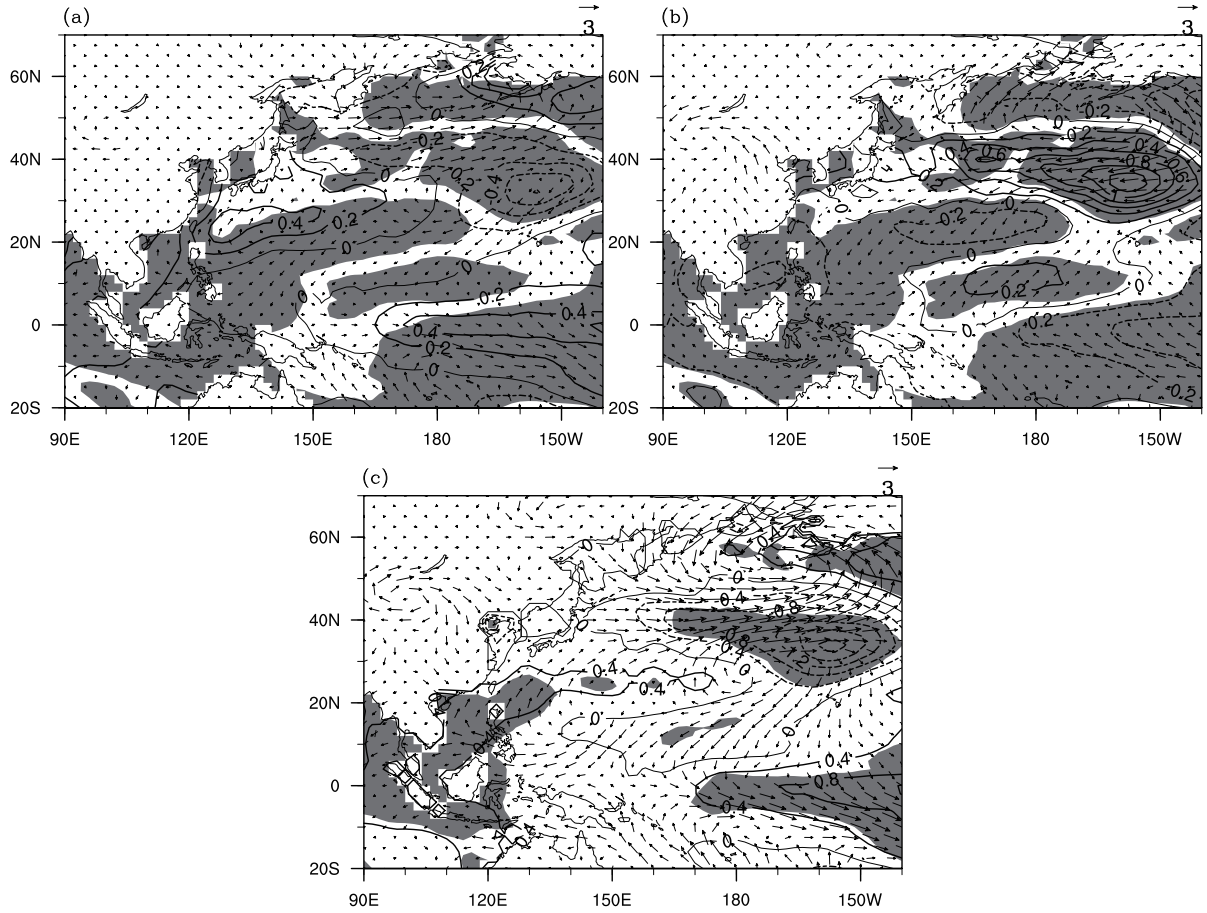

Fig. 4. Composite sea surface wind and temperature anomalies in a typical year with deepened and weakened spring Pacific Aleutian low: (a) deepened, (b) weakened, and (c) deepened minus weakened. Vectors: winds, unit: m s^{-1}; contours: SST anomalies. Dashed lines indicate negative values, shaded area indicate the region of wind anomalies beyond the 95% confidence level. Contour intervals are 0.2, and units are °C.

harmonic waves and low-frequency vorticity oscillation enhanced our knowledge of the low-frequency physical processes that characterizes the major mode configuration of the PPV, NPO, and North Pacific SSTA (the westerly drift zone, ENSO phase), and of their possible impacts on the summer middle and high latitudes atmospheric circulation over Asia.

4.1 *Atmosphere–ocean system configuration in the early phase of cool summers in Northeast China*

In Table 1, a large difference between two individual years (1964 and 1993) in terms of the basic atmosphere–ocean system configuration of the early phase and associated seasonal variations can be seen. In the preceding winter, the PPV area index, NPO, and NAO basically remained in opposite phases. Meanwhile, the westerly drift zone and the central and eastern equatorial Pacific SST agreed with one another in phase, though became opposite in the spring. This can be explained by the fact that the preceding winter of 1964 and the following spring also reported the opposite phase of NPO, NAO, westerly drift zone, and central and eastern equatorial Pacific index.

4.2 *Seasonal evolution of atmosphere–ocean system*

4.2.1 500-hPa *height anomalies*

The 500-hPa height anomalies are given in Fig. 5, in the preceding winter of 1964 underwent a typical strong negative phase over the North Atlantic Ocean (a southbound "+, −" wave train from Iceland), and a positive NPO-like phase above the North Pacific (a southbound "−, +" wave train from the Aleutian Islands) can be seen. In the spring, NAO remained in the negative phase, though significantly weak, with the North Pacific turning into a significant negative phase (a southbound "−, +" wave train from the south). Positive anomalies started to occupy the entire middle and high latitudes across the North Pacific, with the strongest center over the Northern Hemisphere. In the

Table 1. Seasonal evolution of indexes in 1964 and 1993.

		Last winter	Spring	Summer
PPV area index	1964	−1.8	−20.6	17.2
(anomaly)	1993	4.3	24.7	9.2
NPO index	1964	0.67	−0.3	0.44
	1993	0.1	0.1	−1.19
NAO index	1964	−0.76	0.9	−0.62
	1993	1.41	−0.1	0.52
ENSO	1964	0.81	−0.4	−0.67
	1993	0.28	0.84	0.47
Westerly drift index	1964	−0.36	0.64	0.40
	1993	−0.29	−1.18	−1.9

summer, NAO continued at its weak negative status. However, it was very difficult to determine the NPO phase status, positive or negative, at middle and high latitudes, as the southbound "−, +" wave train has moved to Northeast Asia from the south. A positive 500-hPa height anomaly stretched from the Laptev Sea to northern Kamchatka Peninsula via the East Siberian Sea from the south. Negative anomalies covered the mid-latitudes in Asia and their southern neighbors, placing the southern part of the Sea of Okhotsk, Northeast China, and southern Yakutsk under the influence of the same negative anomalies. Meanwhile, a weak positive anomaly (Figs. 5a–c) prevailed over the Ural Mountains in the north. In the preceding winter, and in the spring and summer of 1993, both NAO and NPO registered a phase evolution opposite that of 1964. In the preceding winter, NAO was in a positive phase enjoying a southeast bound "+, −" wave train over Iceland from the northwest, while NPO remained in an atypical negative phase. In the spring, NAO was atypically positive in phase, exhibiting a southwest-bound "−, +" wave train from the northeast, with NPO in a strong positive phase. The negative anomalies above the Aleutian Islands swept across the entire middle and high latitudes in the North Pacific, with its central value at its lowest over the Northern Hemisphere. In the summer, both NAO and NPO were positioned in a significantly weakened negative phase, with strong positive anomalies running from the Asian Ural Mountains in the north to Novaya Zemlya, suggesting that the blocking was particularly strong in western Asia, with a relatively weak positive anomaly blocking over a stretch from Lake Baikal to the Sea of Okhotsk. As a result, the Eurasian mid-latitudes were prevailed upon by negative anomalies, and a vast region from Northeast China to 30°N and the northwestern Pacific were dominated by −20 gpm negative anomalies (Figs. 5d–f).

Apparently, Northeast Asia mid-latitudes were dominated by significant negative anomalies, despite the fact that 1964 and 1993 had somewhat different atmosphere–ocean mode configurations and seasonal evolutions in the early stages, and that the summer of 1964 was prevailed upon by Northeast Asian high-latitude blocking and the summer of 1993 a western Asian mid- and high-latitude blocking.

4.2.2 *SST anomalies*

Figure 6 depicts the seasonally averaged SST anomalies over the North Pacific. In 1964 the SSTA over the North Pacific westerly drift zone changed from the eastbound "−, +" wave train featuring a vague warm or cold phase in the preceding winter into an abruptly enhanced spring warm phase that sustained and further enhanced into the summer. In the preceding winter, the central and eastern equatorial Pacific SSTA remained in a pattern that featured a weak warm phase for the central Pacific and a weak cold phase for the eastern Pacific. The pattern was transformed into a consistent strong La Niña phase in the spring that continued into the summer. In the preceding winter of 1993, the North Pacific westerly drift zone SSTA was warm in the northwest and cold in the southeast. The SSTA underwent a cold phase in the spring and a noticeable cold phase in the summer. Meanwhile, the central and eastern equatorial Pacific SSTA changed from a weak warm phase in the preceding winter to a strong El Niño phase in the spring, proceeding into a noticeably weakened warm phase in the summer.

4.3 *Harmonic waves and LFOs*

4.3.1 500-hPa *ultra-longwave and longwave activities*

Figure 7 shows the 500-hPa ultra-longwave perturbation along 45°N from April to July. During the period April–May 1964, the Northwest Pacific mostly underwent a mobile longwave trough and ridge, rather than a stable ultra-longwave trough above its central and western parts. The situation changed starting at the end of May, when a relatively sta-

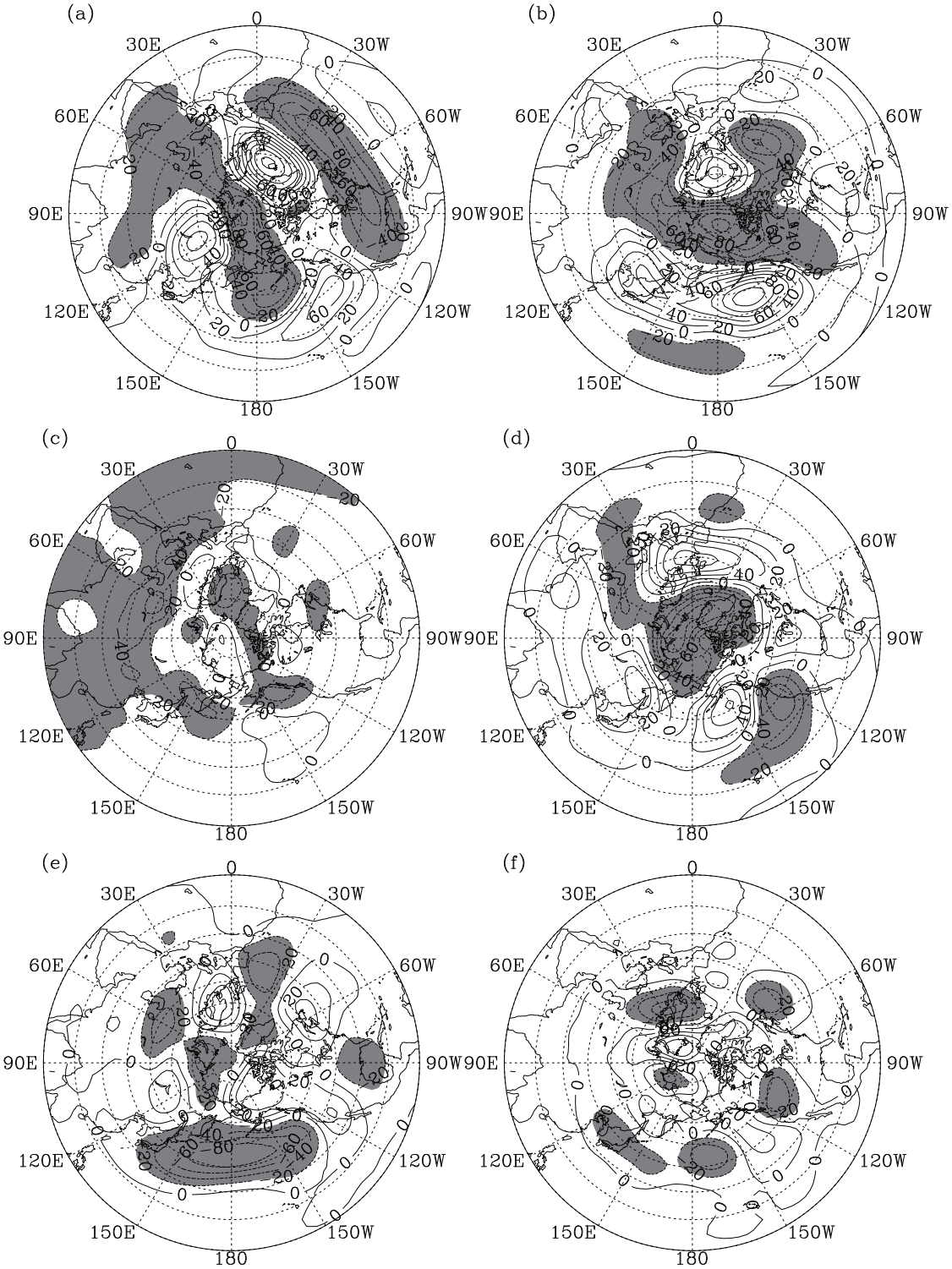

Fig. 5. Seasonally averaged 500-hPa height anomalies: (a) the preceding winter, (b) the spring, and (c) the summer of 1964; and (d) the preceding winter, (e) the spring, and (f) the summer of 1993. Shaded areas are for $\leqslant -20$. Contour intervals are 20, and units are gpm.

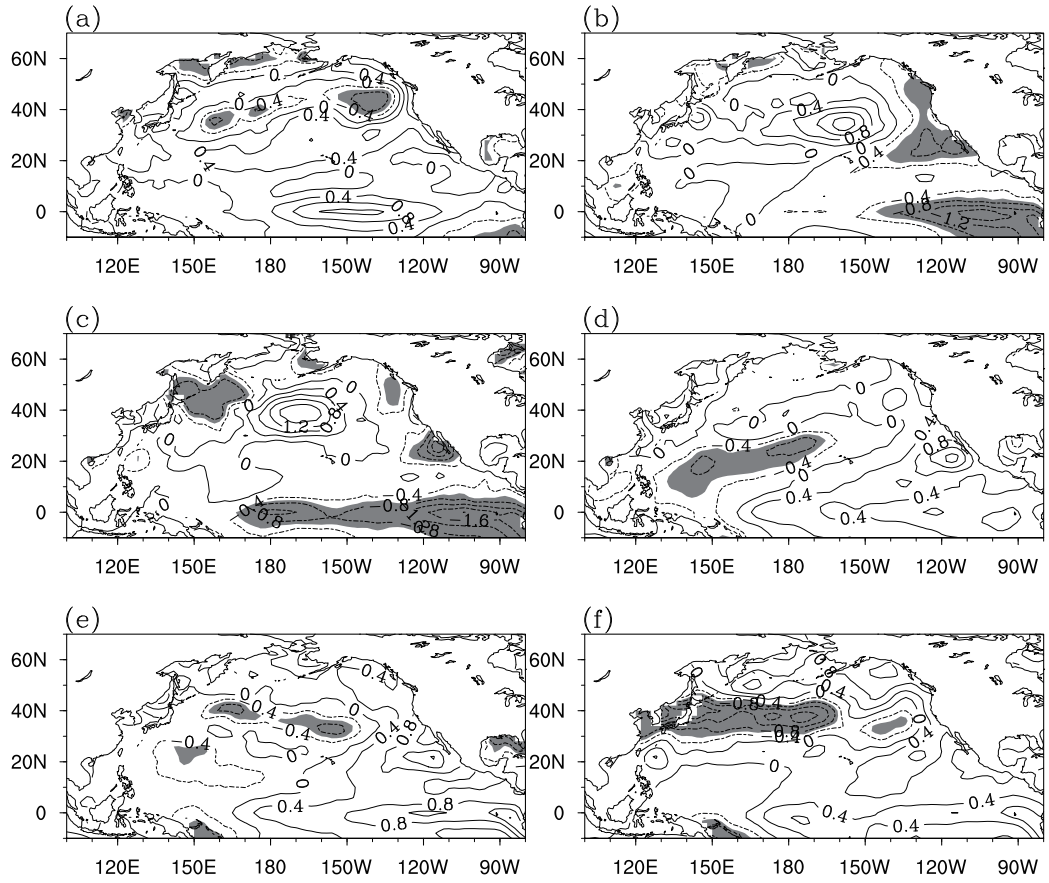

Fig. 6. Seasonally averaged SST anomalies in the Northern Hemisphere: SSTA in (a) the preceding winter, (b) the spring, and (c) the summer of 1964, and SSTA in (d) the preceding winter, (e) the spring, and (f) the summer of 1993. (Dashed lines are for negative values, and shaded areas are for SSTA $\leqslant -0.6$. Contour intervals are 0.2, and units are °C.)

ble super-longwave disturbance trough appeared, retreating westward and wandering over an area west of 120°E in June–July (Fig. 7a, thick arrows). During the period April–July 1993, except the first half of June, the slow eastbound movement of the upstream ultra-longwave disturbance confined the western boundary of the trough influence east of 130°E, though the trough made a rapid west-bound advance in the second half of June, dominating the areas near 120°E. As a result, the central and western parts of the northwestern Pacific (Fig. 7b, 120°E–150°W, thick arrows) was solidly occupied by a stable ultra-longwave disturbance trough.

Figure 8 shows the 500-hPa ultra-longwave perturbation along 65°N from April to July. In late May 1964, an ultra-longwave disturbance ridge that originated from the central and eastern Pacific started to scale back to an area near 120°E. The same movement occurred twice in June–July (Fig. 8a, thick arrows). In mid-June 1993, a noticeable ultra-longwave ridge that originated from the central and eastern Pacific retreated to an area near 120°E (Fig. 8b, thick arrows).

4.3.2 500-hPa *vorticity and associated* 30–60-*d LFO*

Figure 9 illustrates the time–longitude sections of 30–60-day vorticity at 500 hPa along 45°N from April to August. In the first half of June, the northeast cold vortex activity area (45°N, 125°E) saw the eastbound low-frequency vorticity originated from 100°E in 1964 (Fig. 9a, thick arrows) and the westbound low-frequency vorticity stemmed from 160°E in 1993 (Fig. 9b, thick arrows). In the same manner, Fig. 10, where the time–latitude sections of 30–60-day vorticity at 500 hPa along 125°E from April to August were given, shows that in most of June, a northbound positive low-frequency vorticity that originated from 15°–25°N appeared in 1964 (Fig. 10a, thick arrows), and a

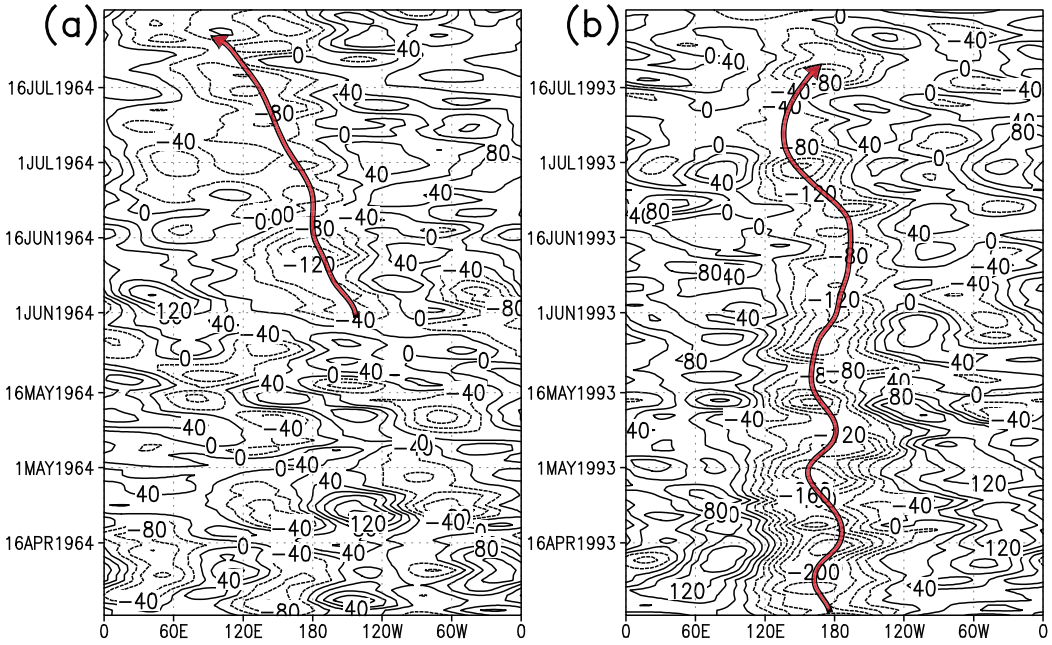

Fig. 7. 500-hPa ultra-longwave perturbation along 45°N from April to July. Thick arrows represent the propagation of the low frequency: (a) 1964 and (b) 1993 (gpm).

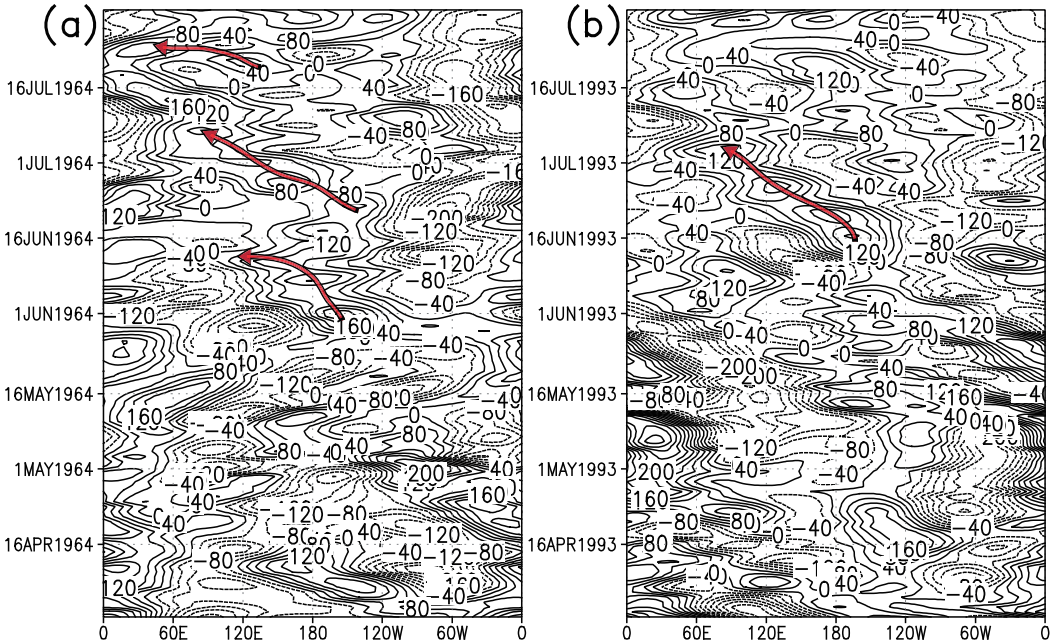

Fig. 8. 500-hPa super-longwave perturbation along 65°N from April to July. Thick arrows represent the propagation of the low frequency: (a) 1964, and (b) 1993 (gpm).

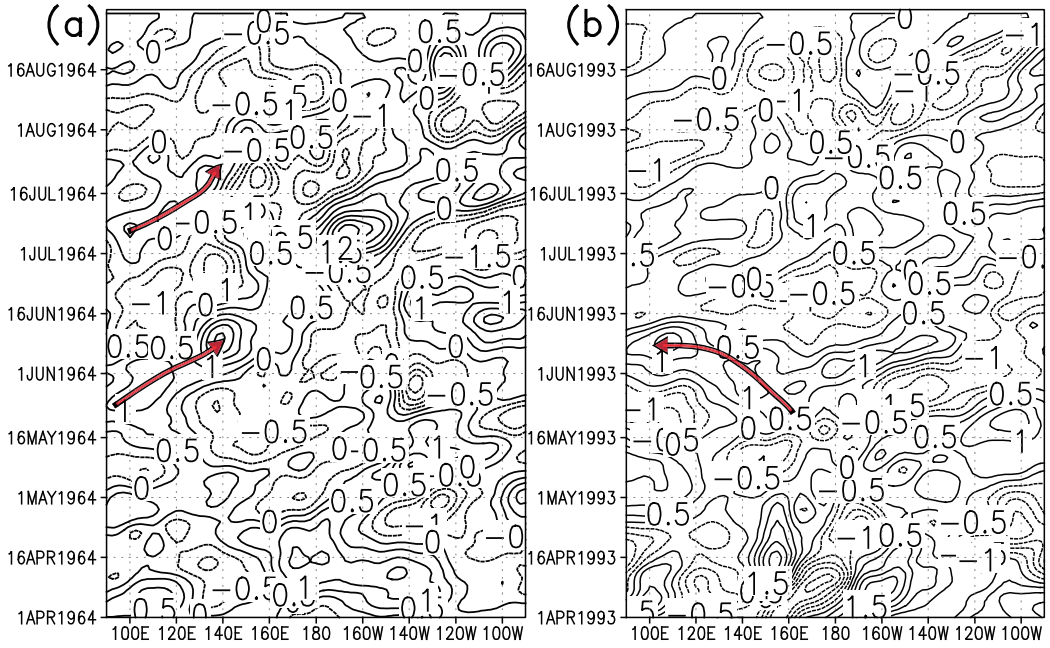

Fig. 9. Time–longitude sections of 500-hPa 30–60-day vorticity along 45°N from April to August (10^{-5} s^{-2}). Thick arrows represent the propagation of the low frequency: (a) 1964 and (b) 1993.

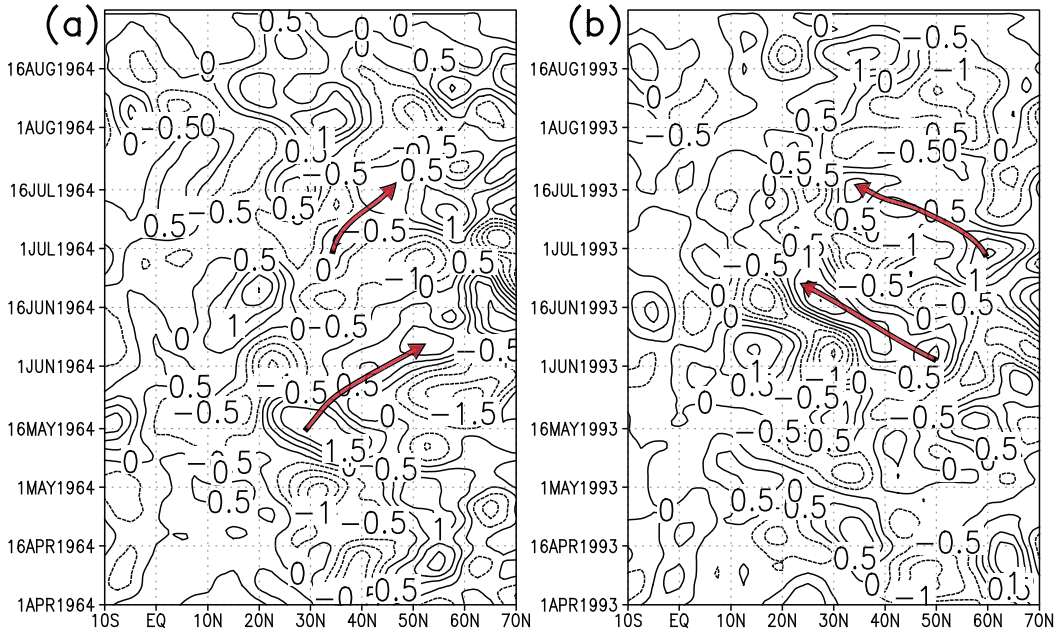

Fig. 10. Time–latitude sections of 500-hPa 30–60-day vorticity oscillation along 125°E from April to August (10^{-5} s^{-2}).Thick arrows represent the propagation of the low frequency: (a) 1964 and (b) 1993.

southbound negative low-frequency vorticity that originated north of 50°N turned up in 1993 (Fig. 10b, thick arrows). This above analysis indicates that 1964 and 1993 registered a vorticity propagation in reverses direction, regardless of longitudinal or zonal orientation.

5. Rossby waves and abnormal summer dipole

The preceding two sections discuss the relationship between a strong or a weak PPV in the spring and a positive or a negative NPO phase, as well as associated North Pacific SSTA (cold or warm westerly drift zone and ENSO phase). The configuration resulted in a strong PPV in the spring of 1993 and a weak PPV in the spring of 1964. As a typical case, both of them contributed to the unusually cool summer events in Northeast China. The configuration also caused a 30–60-d LFO to the 500-hPa height anomaly field, ultra-longwave, longwave and vorticity, and defined the seasonal and monthly evolution pattern of SST anomalies. To further understand the northeast cold vortex, a system having a direct bearing on the summer low-temperature events in Northeast China, and the sustained abnormal activities of the Asia blocking high (dipole), a major system that has an impact on summer low-temperature events, this section discusses the Rossby wave energy dispersion process reported in April–June of 1964 and 1993, to establish a connection between the dipole and early summer circulation anomalies and to sort out their possible wave sources (Bueh and Nakamura, 2007).

Figure 11 shows the 500-hPa circulation anomalies and the corresponding wave action in April–June of 1964 and 1993. To compare the circulation anomalies at different latitudes, the figure also shows geopotential height anomalies in the form of stream functions (i.e., geopotential height anomalies multiplied by $\sin 45°/\sin\varphi$, where φ represents latitude). Comparisons among Figs. 11a–f indicate that a "$-,+,-$" height anomaly wave train appeared over an area stretching from the 500-hPa polar area to the North Pacific, and from East Asia to North America, in the April of 1964, and a "$+,-,+$" height anomaly wave train appeared over this region in 1993. The wave sources were basically positioned over the North Pacific region in 1993 (Fig. 11d). In 1964, the wave sources were positioned mainly over East Asia, with the strongest wave source near the western coast of North America (in Fig. 11a, the light gray area represents the largest combined area). No large variations of height anomaly wave train occurred in the May months of both 1964 and 1993 in the polar sector and in the North Pacific. However, in 1964, the polar sector registered a negative anomaly, with AO in a typical positive phase. Meanwhile, the Aleutian low weakened noticeably again, allowing the positive anomalies to sweep across the North Pacific with a center in the south of the Aleutian Islands. The positive anomalies enhanced rapidly, with the central value reaching 160 gpm, and they became the strongest wave source and sink at middle and high latitudes over the Northern Hemisphere (Fig. 11b). The wave action was basically northerly and southerly in distribution, either pointing to the equator above the northwestern Pacific or moving toward the pole over the northeastern Pacific. In May 1993, the positive polar anomalies left AO in a typical negative phase. At that moment, both wave source and sink displayed a large variation in distribution, mainly over the western coast of North America, or near Great Britain east of the North Atlantic (Fig. 11e). In June 1964, the strongest positive anomaly zone in the Northern Hemisphere was found in an area stretching from the Aleutian Islands to the north of the Kamchatka Peninsula, accompanied by wave sources. The positive anomaly zone was apparently the result of the northwestward retreat of the positive anomalies across the North Pacific with a center in the south of the Aleutian Islands in May 1964 (the Rossby wave action flux in early, mid, and late June 1964 makes a further evidence, though not shown in the figure). In the south of the anomalies sat a vast negative anomaly zone, a typical dipole anomaly pattern in Northeast Asia (Fig. 11c). In June 1993, the most significant positive anomalies prevailed over an area in the north of the Ural Mountains, constituted the west blocking in Asia, which could mostly be the result of the eastbound shift of the positive anomalies that wandered above the Scandinavian Peninsula in May 1993 (Fig. 11f). The Rossby wave action flux in early, mid, and late June 1993 makes a further evidence to support the scenario (not shown in the figure). It can be seen from Tables 2 and 3 that the June and summer of 1964 was prevailed upon by the east blocking and abnormally increased northeast cold vortex days in Asia, which defined a typical Northeast Asia dipole configuration (Fig. 11c). However, in the June and summer of 1993, the Ural blocking high (west blocking) prevailed, and abnormally increased northeast cold vortex days, which constituted another Asia dipole configuration (Fig. 11f).

6. Decadal variation background of 1964–1993 spring polar vortex area index

Figure 12 depicts the opposite variation trends of the PPV area index (green line) and the polar vortex index in other Northern Hemisphere regions in the spring seasons of 1948–2009. The Mann-Kendall (M-

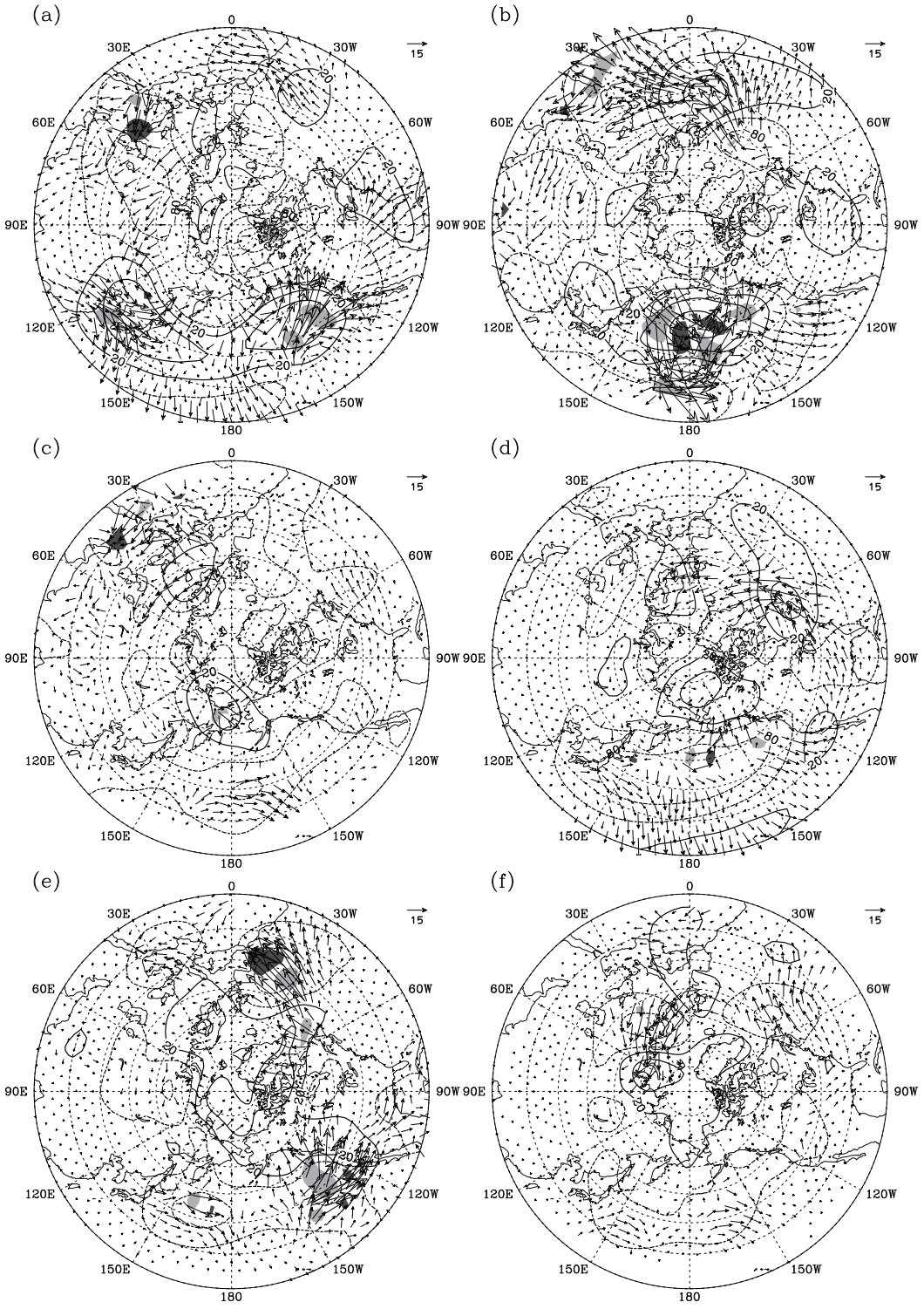

Fig. 11. 500-hPa geopotential height anomalies (gpm, contours) from April to June and associated wave action flux (arrows).Contours are set at ±20, ±80, and ±160 gpm, respectively. Dashed lines represent negative values. Light shading indicates wave action flux divergence that is $> 2\times10^{-5}$ m s^{-2} area. Dark shading indicates wave action flux convergence that is $< -2\times10^{-5}$ m s^{-2} area: (a) April, (b) May, and (c) June of 1964, and (d) April, (e) May, and (f) June of 1993.

Table 2. Number of blocking high days in the June of 1964 and 1993. (units: d)

		Easterly	In-the middle	Westerly	Others
1964	June	16	0	0	14
	Early	8	0	0	0
	Mid	8	0	0	10
	Late	0	0	0	4
1993	June	12	12	12	13
	Early	3	12	6	7
	Mid	0	0	6	0
	Late	9	0	0	6

Table 3. Summer blocking high and abnormally increased northeast cold vortex days in 1964 and 1993. (units: d)

	Blocking high			NCV activities (anomaly)
	East	Central	West	
1964	+6.4	−12.5	−4.7	52 (+13)
1993	−3.6	−11.5	+5.4	46 (+7)

K) method was used to test the point mutation, which indicated that the former underwent an abrupt change in the late 1960s (Fig. 12b) that was noticeably different from the one reported by other regions. The PPV saw a noticeable decline in the spring of 1964, while the same indicator saw a noticeable boost in the spring of 1993. In Fig. 12a, one can see that five polar vortex index curves ended up in a continued downward trend heading to 2009.

7. Discussion and conclusion

(1) In this study, the composite anomalies and SVD method were employed to reveal the major mode configuration of the PPV, NPO, and North Pacific SSTA (westerly drift zone, ENSO phase), in an attempt to sort out the strong and weak spring PPV area that may contribute to positive and negative NPO phase anomalies at the mid-troposphere and in the sea-level pressure fields. Meanwhile, positive or negative NPO phase anomalies often agreed with the first coupled mode that enjoys a stable cold or warm westerly drift zone SST phase and an equally stable El Niño or La Niña phase (e.g., SVD1 accounted for 60% of the squared covariance and total contribution). This conclusion was further confirmed by the combined sea surface wind and temperature anomalies in a typical year, with deepened or weakened spring Pacific Aleu-

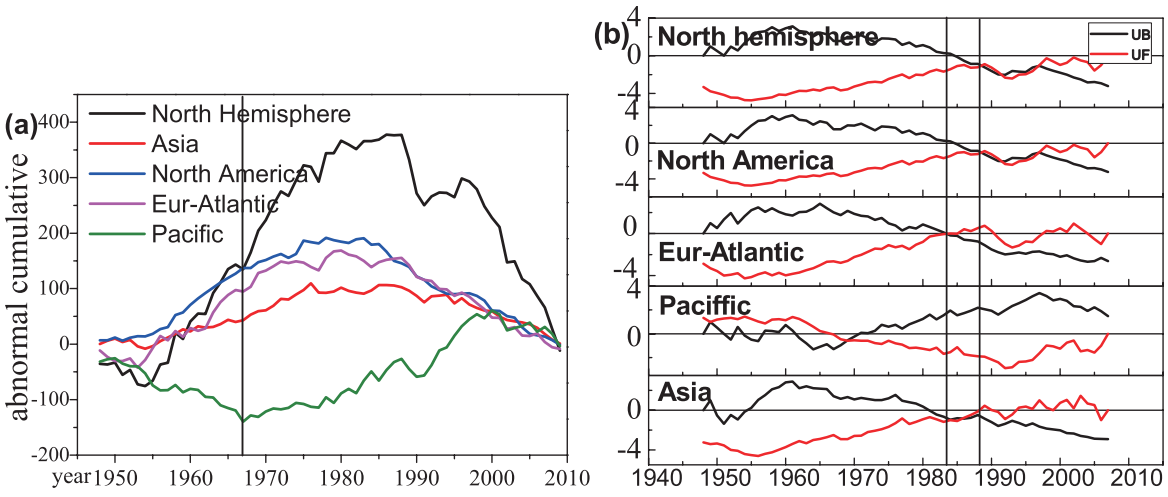

Fig. 12. (a) Combined spring polar vortex area index anomalies, and (b) M-K tests.

tian low.

(2) The year 1964, with a high cool summer incidence, and the year 1993, with a low cool summer incidence, were different only in basic atmospheric mode configuration, and their major North Pacific SST phases were similar. Compared with the preceding winter, the spring of 1964 included a reversed phase realignment of the PPV index, NPO/NAO, westerly drift zone, and the central and eastern equatorial Pacific SSTA. However, 1993 was consistent in both the preceding winter and the following spring. As a result, the opposite phases of major atmosphere–ocean system modes in the spring of two individual years would naturally produce a different evolution from the spring to the summer. For example, in the spring of 1964 a very weak PPV occurred, with NPO in a typical negative phase, the westerly drift zone in a strong warm phase, and the central and eastern equatorial Pacific SSTA in La Niña phase. In contrast, in the spring of 1993, the polar vortex was strong, and NPO occurred in a typical positive phase, with the westerly drift zone in a zero phase and the central and eastern equatorial Pacific SSTA in an El Niño phase. Entering the summer, the westerly drift zone was positioned in a noticeably cold phase, and the central and eastern equatorial Pacific SSTA was in a weakened El Niño phase. However, unusually cool summers occurred in both individual years, regardless of the difference between the two. The reversed realignment of basic atmosphere–ocean system modes from the preceding winter to the following spring, creating the "spring forecast threshold."

(3) In this study, diagnoses were conducted to understand the evolution patterns of mid-troposphere harmonic waves, low-frequency vorticity oscillations, and Rossby wave energy, to further reveal the fact that both 1964 and 1993 shared a low-frequency physical process that contributed to the mid- and high-latitude summer dipole circulation anomalies, even though the two individual years exhibited entirely different modes of configuration for spring signal, PPV, NPO, and North Pacific SSTA (westerly drift zone, ENSO phase). However, in the spring of 1964, a weak polar vortex and a typical negative NPO combined with the warm westerly drift zone and the La Niña-oriented central and eastern equatorial Pacific SSTA to create a dominant Okhotsk blocking high (eastern blocking) in the coupled atmosphere–ocean process from the spring to the summer. The northeast cold vortex acquired its positive vorticity mainly from the western path, and from the low-latitude transport as well. However, in the spring of 1993, the strong polar vortex area and positive NPO phase collaborated with the zero phase of westerly drift zone SSTA and the El Niño-oriented central and eastern equatorial Pacific SSTA to stage a Ural blocking high (western blocking), with the northeast cold vortex obtaining its positive vorticity mainly from the westbound retreating ultra-longwave disturbance trough (eastern path) in the central North Pacific, and from high-latitude transport as well.

(4) The PPV index exhibited an opposite variation trend against the polar vortex index in other Northern Hemisphere regions in the spring seasons of 1948–2009. The M-K method was employed to test the point mutation, which indicated that the former registered an abrupt change in the late 1960s that was noticeably different from the one reported by other regions. The PPV area noticeably declined in the spring of 1964, while the same indicator noticeably enhanced in the spring of 1993. The pattern revealed from a different perspective that both 1964 and 1993 underwent an unusually cool summer in Northeast China, regardless of the large difference between the two in early basic atmosphere–ocean mode configuration and in seasonal evolution. On one hand, the two individual years, either as a high incidence or as low incidence years, had different configurations of early signals and summer dipole, which could probably be explained by the difference in interdecadal variation. On the other hand, both 1964 and 1993 shared a low-frequency physical process that contributed to the mid- and high-latitude summer dipole circulation anomalies.

In this study, only the spring polar vortex area anomalies in four typical strong and four typical weak years, and the basic patterns of abnormal phase couplings between NPO and the North Pacific westerly drift zone and the central and eastern equatorial Pacific SSTA were analyzed. The years 1964 and 1993, where a significant cool summers occurred in Northeast China, were chosen to represent typical years of a weak or a strong PPV area corresponding to a high or a low cool summer incidence. The two individual years were simply opposite in phase anomalies, in terms of polar vortex area, NPO, the westerly drift zone, and the central and eastern equatorial Pacific SSTA. The significant difference, as such, probably represents the major footprints of interdecadal variations of summer low-temperature events in the northeast. Some other points, including early signals and atmosphere–ocean coupling processes in a typical low- or high-incidence year and their applicability to other individual years, require further study.

Acknowledgements. This work was jointly supported by the National Natural Science Foundation of China (Grant Nos. 41175083 and 41275096), and the Special Fund for Meteorological Scientific Research

in the Public Interest (Grant Nos. GYHY201006020, GYHY201106016, and GYHY201106015).

REFERENCES

Bjerknes, J., 1966: A possible response of the atmospheric Hadley circulation to equatorial anomalies of ocean temperature. *Tellus*, **18**, 820–829.

Bjerknes, J., 1969: Atmospheric teleconnection from the equatorial Pacific. *Mon. Wea. Rev.*, **97**, 163–172.

Bueh, C. L., and H. Nakamura, 2007: Scandinavian pattern and its climatic impacts. *Quart. J. Roy. Meteor. Soc.*, **133**, 2117–2131.

Chou, Y. Y., 1985: *Medium Term Weather Forecast*. Science Press, Beijing, 920pp. (in Chinese)

Demmel, J., and W. Kahan, 1990: Computing small singular values of bidiagonal matrices with guaranteed high relative accuracy. *SIAM Journal on Scientific and Statistical Computing*, **11**, 873–912.

Huang, R. H., and W. J. Li, 1987: Influence of heat source anomaly over the western tropical Pacific on the subtropical high in East Asia. *Paper presented at International Conference on the General Circulation of East Asia,* Chinese Academy of Science, Chengdu, China, 10–15 April.

Huang, R. H., and W. J. Li, 1988: Heat source anomalies over the western tropical Pacific in the summer and its impacts on the East Asia subtropical high and associated physical mechanism. *Scientia Atmospherica Sinica*, **12**(9), 107–106. (in Chinese)

Huang, R. H., and F. Y. Sun, 1992: Impacts of the tropical western Pacific on the East Asian summer monsoon. *J. Meteor. Soc. Japan*, **70**(1), 243–256.

Klein, W. H., 1952: Some empirical characteristics of long waves on monthly mean charts. *Mon. Wea. Rev.*, **80**, 203–219.

Li, C. Y., 1989: El Niño events and temperature anomalies in eastern China. *Journal of Tropical Meteorology*, **3**, 210–219. (in Chinese)

Li, C. Y., 1990: Intraseasonal oscillation in the atmosphere. *Scientia Atmospherica Sinica*, **14**, 32–45. (in Chinese)

Li, J., and J. Wang, 2003: A new North Atlantic Oscillation index and its variability. *Adv. Atmos. Sci.*, **20**(5), 661–676.

Lian, Y., 2007: Correlation between North Pacific oscillation and East Asian summer monsoon. *Scientia Geographica Sinica,* **27**(Suppl.), 19–27. (in Chinese)

Lian, Y., and G. An, 1998: The relationship among East Asia summer monsoon El Nino and low temperature in the Songliao plains Northeast China. *Acta Meteorologica Sinica*, **56**, 724–734. (in Chinese)

Lian, Y., C. L. Bueh, Z. W. Xie, and F. S. Li, 2010: The anomalous cold vortex activity in Northeast China during the early summer and the low-frequency variability of the Northern Hemispheric atmosphere circulation. *Scientia Atmospherica Sinica*, **34**, 429–439. (in Chinese)

Liang, F., S. Y. Tao, J. Wei, and C. L. Bueh, 2011: Variation in summer rainfall in North China during the period 1956–2007 and links with atmospheric circulation. *Adv. Atmos. Sci.*, **28**, 363–374, doi:10.1007/s00376–010–9220–2.

Liu, G., B. Z. Shen, Y. Lian, S. F. Li, L. Cao, and P. Liu, 2012: The sorts of 500 hPa blocking high in Asia and it's relations to cold vortex and aestival low temperature in northeast of China. *Scientia Geographica Sinica*, **32**, 1269–1274. (in Chinese)

Liu, Z. X., 1986: Calculation of the intensity of the northern hemisphere polar vortex area index and its association with temperature variations in China. *Meteorological Monthly*, **2**(Suppl.), 84–89. (in Chinese)

Liu, Z. X., Y. Lian, Z. T. Gao, L. Sun, and B. Z. Shen, 2002: Analyses of the Northern Hemisphere circulation characters during northeast cold vortex persistence. *Scientia Atmospherica Sinica*, **26**, 361–372. (in Chinese)

Liu, Z. X., Y. Lian, B. Z. Shen, Z. T. Gao, and X. L. Tang, 2003: Seasonal variation features of 500 hPa height in North Pacific oscillation region and its effect on precipitation in Northeast China. *Journal of Applied Meteorological Science*, **14**, 553–561. (in Chinese)

Madden, R. D., and P. Julian, 1971: Detection of a 40–50 day oscillation in the zonal wind in the tropical pacific. *J. Atmos. Sci.*, **28**, 702–708.

Madden, R. D., and P. Julian, 1972: Description of global scale circulation cells in the tropics with 40–50 day period. *J. Atmos. Sci.*, **29**, 1109–1123.

Namias, J., 1951: The great Pacific anticyclone of the winter 1948–50: A case study in the evolution of climatic anomalies. *J. Meteor.*, **8**, 251–261.

Mantua, N. J., S. R. Hare, Y. Zhang, J. M. Wallace, and R .C. Francis, 1997: A Pacific interdecadal climate oscillation with impacts on salmon production. *Bull. Amer. Meteor. Soc.*, 78, 1069–1079.

National Climate Center, 2010: *2009 Annual Report on Climate System Monitoring and Diagnosis*. China Meteorological Press, Beijing, 176pp. (in Chinese)

Peng, S. Q., and J. J. Zhang, 1998: The statistical diagnosis and numerical experiment of atmospheric teleconection patterns in Northern Hemisphere. *Journal of Applied Meteorological Science*, **9**, 65–71. (in Chinese)

Rogers, G. T., 1981: The north-Pacific oscillation. *J. Climate*, **1**, 68–83.

Shen, B. Z., S. Liu, Y. Lian, G., L. Feng, S. F. Li, and Z. Q. Gong, 2011: An investigation into 2009 summer low temperature in Northeast China and its association with prophase changes of the air-sea system. *Acta Meteorologica Sinica*, **69**, 320–333. (in Chinese)

Sun, J. Q., and H. J. Wang, 2006: Regional difference of summer air temperature anomalies in Northeast China and its relationship to atmospheric general circulation and sea surface temperature. *Chinese Journal of Geophysics*, **49**, 662–671. (in Chinese)

Wallace, J. M., and D. S. Gutzler, 1981: Teleconnections in the geopotential height field during the Northern

Hemisphere winter. *Mon. Wea. Rev.*, **109**, 784–812.

Yang, H., and S. Q. Sun, 2005: The characteristics of longitudinal movement of the subtropical high in the Western Pacific in the pre-rainy season in China. *Adv. Atmos. Sci.*, **22**, 392–400.

Yang, Q., Y. Lian, and J. H. He, 2005: Predicting northeast cool summer using singular value decomposition method. *Meteorological Monthly*, **31**, 31–35. (in Chinese)

Zhang, S. Q., 1990: Cold Temperature in Northeast China and its association with El Niño. No. 5, *China Science and Technology Blue Book*, National Science and Technology Commission, China Science and Technology Press, 308–310. (in Chinese)

Zhang, S. Q., T. J. Yu, F. Y. Li, X. M. Wang, X. F. Wang, and W. M. Wu, 1985: Seasonal variation of Northern Hemisphere polar vortex area and associated intensity, and their association with the temperatures in Northeast China. *Scientia Atmospherica Sinica*, **9**, 178–185. (in Chinese)

Zhao, Z. G., and Q. S. Liao, 1992: Winter North Pacific oscillation and summer rainfall in China. *Meteorological Monthly*, **18**, 11–16. (in Chinese)

Zheng, W. Z., and Y. Q. Ni, 1999: Tropical and midlatitude Pacific SSTA and its impacts on summer low temperature stress in East Asia. *Journal of Applied Meteorological Science*, **10**, 394–401. (in Chinese)

Zhou, B. T., H. J. Wang, and X. Cui, 2008: Significant relationship between Hadley circulation and North Pacific Oscillation. *Chinese Journal of Geophysics*, **51**, 999–1006. (in Chinese)